

Abstract

HAMPTON, AUSTIN SCOTT. Linking Mechanics and Energetics of Post-Stroke Walking: Towards a Muscle-Level Understanding. (Under the direction of Gregory S. Sawicki, Michael Lewek, Peter Mente, and Andrew DiMeo).

Post-stroke walking is characterized by an asymmetrical walking pattern and typically costs more metabolic energy. Though many researchers have performed thorough investigations of post-stroke gait, it is still unclear what factors may be contributing to this higher metabolic demand, especially at the joint and muscle levels.

In this study, we performed an inverse dynamics analysis on the gait pattern of participants who had a stroke walking at 0.75 m s^{-1} and compared to unimpaired controls. We wanted to further elucidate the mechanisms that cause the asymmetry and weakened ankle push-off seen in post-stroke walking and determine if there is a link to an increased metabolic cost. Our results indicate the metabolic cost was 51% higher post-stroke when compared to controls. We also found the combined (paretic + non-paretic) average positive mechanical power for the lower limb was increased by 34% for the participants when compared to non-disabled controls. There was more reliance on the hip to compensate for the weak ankle joint and produce the additional lower limb work. We believe that combining the increase in hip power production and estimates for hip joint apparent efficiency can help explain the increase in metabolic cost.

We further ‘zoomed’ in on the ankle joint to determine if the musculo-tendon interactions are disrupted post-stroke by combining an inverse dynamics analysis with real-time ultrasound images. In unimpaired gait, the ankle joint utilizes a catapult mechanism with the Achilles tendon to produce efficient elastic power. To our surprise, though, there were few differences in kinetics and kinematics of the muscle-tendon unit (MTU), series elastic

element (SEE), and contractile element (CE) post-stroke. One notable finding was additional lengthening and energy absorption done by the non-paretic fascicles (CE). Despite these differences in absorption, the catapult mechanism was not significantly altered and adequate amounts of forces were produced.

This information could be used to aid in the design of rehabilitative regimes or assistive devices used in therapies for pathological gaits. Therapies could focus on improving flexibility and strength of the paretic ankle joint. Also, this study shows the importance of designing devices that can help unload the additional work load done by the hip joint post-stroke.

© Copyright 2012 by Austin Hampton

All Rights Reserved

Linking Mechanics and Energetics of Post-Stroke Walking: Towards a Muscle-Level
Understanding

by
Austin Scott Hampton

A thesis submitted to the Graduate Faculty of
North Carolina State University
in partial fulfillment of the
requirements for the degree of
Master of Science

Biomedical Engineering

Raleigh, North Carolina

2012

APPROVED BY:

Gregory Sawicki,
Committee Chair

Dr. Michael Lewek

Dr. Peter Mente

Dr. Andrew DiMeo

Biography

Austin is a Master of Science candidate in the joint Biomedical Engineering Program at North Carolina State University and the University of North Carolina – Chapel Hill. He graduated magna cum laude from North Carolina State University in 2010 with his Bachelor of Science in Biomedical Engineering (BSBmE) with an emphasis in biomechanics. In addition to his current field of study, he also conducted research in the field of osseointegrated prosthetics focusing on the skin/bone/device interface under the tutelage of Dr. Ola Harrysson. He is a member of the Tau Beta Pi engineering honor society, and outside the world of academia, Austin was a division-I varsity scholarship athlete for the North Carolina State Wolfpack. He is the current record holder on the 3-meter event, achieved All-ACC honors in athletics, and received a post-graduate scholarship from the ACC to further his education.

Acknowledgements

I would like to first acknowledge my family for making sacrifices and encouraging me to be the best. Without their support and love, my athletic and academic achievements would not have been possible. Next, I would like to thank my adviser Dr. Gregory Sawicki for his backing and guidance throughout this whole process. He has truly been a wonderful mentor and friend, and I owe a lot to him. Also, Dr. Michael Lewek has greatly aided in the recruitment of the participants, which made this study possible. Additionally, I would like to extend my upmost gratitude to Dr. Dominic Farris for his assistance in the data collections and data analysis. Lastly, I would like to acknowledge my friends I have here in Raleigh, North Carolina. Their unconditional love and care through one of the most personally difficult and professionally challenging time periods in my life is irreplaceable and has been one of the major reasons I have been able to finish.

*** This work was partially funded by grant award #50KR1018 to GSS from the UNC-based North Carolina Translational and Clinical Sciences Institute (TraCS).

Table of Contents

List of Tables	v
List of Figures	vi
Linking Mechanics and Energetics of Post-Stroke Walking: A Joint-Level Perspective	1
Introduction.....	1
Materials and Methods.....	4
Results.....	9
Discussion.....	10
Conclusions.....	15
Medial Gastrocnemius Muscle Behavior During Post-Stroke Walking.....	17
Introduction.....	17
Materials and Methods.....	20
Results.....	25
Discussion.....	29
Overall Conclusions and Future Directions.....	33
References.....	36
Appendices.....	41
Appendix A – Tables	42
Appendix B – Figures.....	45

List of Tables

Appendix A – Tables	42
Table 1: Listing of participant characteristics.....	42
Table 2: Average positive and negative powers (W kg-1) for the hemiparetic and the non-disabled control participants.....	43
Table 3: Average positive and negative powers (W) for the control, paretic, and non-paretic MTU, CE, and SEE.....	43
Table 4: Maximum force of the MG muscle fascicles (N) for the control, paretic, and non-paretic limbs. Also the percent stride (%), the change in length (mm) and velocity (mm s-1) of the MTU, CE, and SEE all recorded at the point in time of the gait cycle of the maximum force (@ Fmax).....	44

List of Figures

Appendix B – Figures	45
Figure 1: Mean lower-limb joint angles (degrees) for post-stroke hemiparetic and neurologically intact control participants during walking at 0.75 m/s.....	45
Figure 2: Ankle, knee and hip moment (N m-1), angular velocity (degrees s-1), and power (W kg-1).....	46
Figure 3: Total average positive power production for post-stroke hemiparetic and unimpaired control participants during walking at 0.75 m s-1	47
Figure 4: Total average negative power production for post-stroke hemiparetic and unimpaired control participants during walking at 0.75 m s-1	48
Figure 5: Net metabolic power (W kg-1) (mean \pm sd) for unimpaired controls and post-stroke hemiparetic participants during walking at 0.75 m s-1.	49
Figure 6: Placement of the ultrasound probe over the muscle belly of the medial gastrocnemius muscle	50
Figure 7: Ankle powers (W kg-1), moments (N*m kg-1), and angular velocities (degrees sec-1) for the paretic, non-paretic, and control limbs over a full stride.....	51
Figure 8: Length-change patterns (mm) of a unimpaired control muscle-tendon unit (MTU), fascicle (CE), and series elastic element (SEE)	52
Figure 9: Length-change pattern (mm) of the MTU, CE and SEE for the paretic, non-paretic and control MG.	53
Figure 10: Force (N), velocity (mm s-1) and power (W) of the MTU, CE and SEE for the control, paretic and non-paretic MG.....	54
Figure 11: Average combined positive and negative power (W) for the CE and the SEE of the control, paretic and non-paretic limb.....	55

Linking Mechanics and Energetics of Post-Stroke Walking: A Joint-Level Perspective

Introduction

A stroke can be an extremely debilitating occurrence that affects approximately 7,000,000 people in the United States¹ and can severely limit mobility. Impaired muscle coordination and reduced muscle strength post-stroke typically result in a walking gait that is asymmetrical and slower than normal²⁻⁵. The walking pattern post-stroke has been shown to be different than a non-disabled gait, which utilizes efficient energy production and transfer mechanisms to help minimize the cost of walking^{2-4, 6-10}.

Unimpaired walking exhibits a finely tuned step-to-step transition and utilizes a strong push-off by the ankle joint. In an efficient step-to-step transition, there is simultaneous positive and negative work of equal magnitude by the trailing and leading limbs respectively¹¹. When timed appropriately, the trailing limb positive power generation serves to limit leading limb collisional losses, minimizing energetic cost⁷. The trailing limb ankle joint is the crucial source of mechanical energy powering push-off to help reduce the energy losses when the leading leg impacts the ground⁷. In fact, the ankle joint in non-disabled walkers has been shown to produce nearly half of the total (ankle + knee + hip) positive work summed across the limb^{6, 10}. When trailing limb push-off is disrupted by weak or uncoordinated ankle plantarflexors, increased collisional losses may require additional mechanical and metabolic energy expenditure from other muscles in the lower limb.

Typically, post-stroke gait displays disrupted gait patterns caused by neuromuscular impairments on one side of their body (i.e. asymmetry)^{3-5, 8, 12, 13}. A particularly notable post-

stroke impairment is that the affected (paretic) ankle joint shows weakened plantarflexors and a decreased ability to produce an adequate push-off pre-swing^{4, 5, 8, 12, 13}. In order to compensate for the weak ankle, mechanical power generation is redistributed and mainly transferred to the hip joint^{3, 8, 12, 13}. Because the hip is less efficient in comparison to the ankle^{6, 10}, the heavy reliance on the hip joint post-stroke may contribute to a raised metabolic cost^{6, 10}. The hip joint does not have the long series elastic element seen in the ankle joint, i.e. the Achilles tendon. This leads to a reduced amount of stored elastic energy being returned back into the system and thus requires additional muscle fascicle work and more metabolic energy. In short, because of differences in mechanical efficiency between proximal and distal joints¹⁰ the distribution of mechanical energy across the lower limb may highly impact the amount of metabolic energy required post-stroke.

Many studies have quantified the metabolic cost of post-stroke walking^{4, 9, 14, 15}. It is clear that metabolic energy expenditure for someone who experienced a stroke can be as much as 1.3 to 2 times higher than non-disabled controls at self-selected fast and slow speeds, respectively⁴. Though many studies have looked at the metabolic consumption post-stroke, few have attempted to establish links between joint mechanics and metabolic expenditure between nondisabled walkers and stroke survivors at matched speeds. In fact, we are only aware of a single study that has documented the center of mass (COM) efficiency (COM mechanical power/net metabolic power) of walking post- stroke. Detrembleur et al. reported that the efficiency of hemiparetic walking (20%) was near normal values reported elsewhere for unimpaired controls at self-selected walking speeds⁴. That study did not control walking

speed, did not make within study control/hemiparetic comparison and employed center of mass-based (COM) analyses that likely underestimated the work of the muscle-tendon units (MTU) across the limb due to simultaneous positive and negative work at adjacent joints¹⁶.

Though many studies have addressed the mechanical energy production^{2, 3, 8, 13} and metabolic energy expenditure^{4, 9, 14, 15} in isolation during walking post-stroke, few have combined mechanical and metabolic measurements to elucidate the mechanisms behind elevated metabolic expenditure. The purpose of this study was to link joint-level mechanics and overall metabolic energy expenditure at a fixed walking speed for participants who experienced a stroke and unimpaired controls. We collected simultaneous joint mechanics (control, paretic, and non-paretic limbs) and metabolic energy expenditure data in both unimpaired controls and participants walking at 0.75 m s⁻¹. Based on previous literature, we anticipated an increased net metabolic power (W kg⁻¹) post-stroke^{4, 9, 14, 15}. In addition, we hypothesized that compared to unimpaired controls: 1) the total positive average mechanical power (W kg⁻¹) summed across the joints of both limbs would be higher post-stroke, 2) a larger portion of the average mechanical power would be performed by the hip muscle-tendon units post-stroke, and 3) due to heavier reliance on inefficient hip muscle-tendon units (MTU) the joint-level efficiency (ratio of summed joint positive average mechanical power to net metabolic power) would be lower post-stroke.

Materials and Methods

Experimental Protocol

Eight walkers who had a stroke (participants) and did not use an ankle-foot orthotic (AFO) (mean \pm s.d., age = 58 ± 11 years ; mass = 95 ± 19 kg; height = 1.77 ± 0.06 m) and nine unimpaired controls (controls) (mean \pm s.d, age = 25 ± 5 years; mass = 72 ± 13 kg; height = 1.69 ± 0.16 m) provided us with an institutional review board (IRB) approved consent form to participate in this study. A more in depth listing of subject characteristics is outlined in Appendix A Table 1. All procedures were approved by the University of North Carolina, Chapel Hill and North Carolina State University institutional review boards (IRB) and followed the procedures outlined by the Declaration of Helsinki.

All trials were completed on an instrumented treadmill (BERTEC, Columbus, OH, USA) set to 0.75 m s^{-1} and lasted four minutes. Each participant wore a harness to reduce the possibility for falls or injury. The harness did not supply any body weight support. The participants were discouraged from using the handrails other than for small balance corrections throughout the trials

Kinetics and Kinematics

An eight camera motion analysis system (VICON, Oxford, UK) was used to capture the position of 37 reflective markers attached to the pelvis, right leg, and left leg (modified Cleveland Clinic marker set) at 120 Hertz. Raw marker positions were filtered using a second-order low pass Butterworth filter with a cut-off frequency of 10 Hertz. A static standing trial was captured and the positions of the markers on segment endpoints were used

to calibrate a four segment (comprised of one pelvis, two thighs, two shanks, and two feet) model on both legs for each subject using established inertial parameter¹⁷. Clusters of three to four markers on rigid plates were attached to the pelvis, thigh, and shank segment to track segment motion on both the left and right leg during the trials. For the foot, a cluster of three markers was attached directly to the walker's shoe. Joint angle for the hip, knee, and ankle were computed in three dimensions as the orientation of the distal segment with reference to the proximal segment and differentiated to calculate joint velocities.

The force data was recorded at 120 Hertz during the movement trial at 0.75 m s^{-1} using two force platforms underneath each belt of the instrumented. The subjects were allowed to choose their step frequency and length freely, were allowed to grip the handrail while the treadmill reached the prescribed speed, and were asked to release the handrail once the speed was obtained. Each participant was required to walk with each foot hitting its ipsilateral treadmill belt and force platform to ensure that individual limb was contributing to that leg's calculations in the double support phase of the gait cycle. The raw force analog data were filtered with a second-order low-pass Butterworth filter with a cut-off frequency of 35 Hertz. Inverse dynamic analyses¹⁸ were then used to compute net joint moments, which were multiplied by the calculated joint angular velocities to calculate joint powers for the hip, knee, and ankle joints. Kinematics and kinetics were calculated for the left and the right leg individually for the participants, but for the unimpaired controls symmetry was assumed and the kinetics and kinematics were calculated for the right leg. The calculations of kinetics and

kinematics were performed using a combination of Visual 3-D software (C-Motion Inc., Germantown, MD, USA) and MATLAB (MathWorks, Natick, MA, USA).

Calculation of Positive and Negative Mechanical Work

We used a joint-level approach to calculate mechanical work and power values because it is more closely related to the actual muscular work and power than other methods (e.g. external and internal work)⁶. Total positive and negative average powers were calculated as the sum of work done at each of the lower limb joints divided by the stride time. For this, stride-averaged joint power data (from 0-100% of the gait cycle) for the ankle, knee, and hip were individually integrated with respect to time over discrete periods of positive and negative work using the trapezium method⁶. For each stride at each joint, all values of positive work were summed and all periods of negative work were summed to give an individual joint positive and negative work, respectively. Work represents the work done by joints of the paretic and non-paretic limbs for the participants who had a stroke and the right limb only for the unimpaired control. In order to obtain the work done by the joints in both legs, the paretic and non-paretic work values were summed, and for the controls, assuming symmetry, the right leg values were doubled. Then, individual joint positive mechanical work values were divided by stride time in order to calculate average positive mechanical joint powers (equation 1), where \overline{P}_j^+ , W_j^+ , T_{stride} are the average positive mechanical power at that joint, positive mechanical work at a joint, and average stride time, respectively.

$$\overline{P}_j^+ = \frac{W_j^+}{T_{stride}} \quad (1)$$

Following this, the average positive powers calculated for the ankle, knee, and hip were summed (equation 2) and this value was taken as the total average positive power output, where $\overline{P_{tot}^+}$, $\overline{P_{hip}^+}$, $\overline{P_{knee}^+}$, $\overline{P_{ank}^+}$ are total, hip, knee, and ankle average positive powers, respectively.

$$\overline{P_{tot}^+} = \overline{P_{hip}^+} + \overline{P_{knee}^+} + \overline{P_{ank}^+} \quad (2)$$

Each joint's average positive and negative powers as a percentage were calculated using equation 3, where $J_{\%}$ is the percent value contributed by the individual joint to the total summed average power.

$$J_{\%} = \left(\frac{\overline{P_J^+}}{\overline{P_{tot}^+}} \right) \times 100\% \quad (3)$$

We computed average negative powers for the limbs and joints using the same procedures outlined in equations 1-3, but computed integrals to get mechanical work using the negative portions of the stride-averaged joint powers.

Metabolic Measurement and Efficiency

The flow rates for oxygen and carbon dioxide were recorded using a portable metabolic system (OXYCON MOBILE, VIASYS Healthcare, Yorba Lina, CA, USA). In order to obtain a net metabolic measurement, we used the last two minutes of a four minute standing trial to calculate rate of metabolic energy consumption (watts) while standing. This value was subtracted from the average flow rate during the last two minutes of the four minute walking trials at 0.75 m s^{-1} . A visual inspection of the oxygen consumption rate data confirmed the subjects were at steady-state. Using the Brockway equation¹⁹, the flow rates for oxygen and

carbon dioxide were converted to metabolic power and then normalized to the subject's body mass (W kg^{-1}).

The efficiency of positive mechanical work during walking (η_{work}^+) was calculated by dividing the total summed average positive mechanical power ($\overline{P_{tot}^+}$) by the net metabolic power (P_{net}) for each participant (equation 4).

$$\eta_{work}^+ = \frac{\overline{P_{tot}^+}}{P_{net}} \quad (4)$$

We accounted for the positive work only and neglected the negative work done during stride because the efficiency for the negative work in muscle has been shown to be five times greater than the positive work²⁰ and accounts for a minimal portion of the total metabolic cost. This may lead to minimally erroneous calculations, but this issue should be systematic during all trials given that the total negative and total positive work performed during a stride are equal for level steady-speed movement trials. In addition, the degree of negative work being absorbed and returned into the elastic structures in the muscle (e.g. tendons) is unknown making it difficult to accurately include in the calculation of efficiency.

Statistical Analysis

For each individual, the kinematic and kinetic data were averaged over 8-10 strides. Group means and standard deviations were then computed and, unless otherwise stated, these values are the values represented. To test for differences in outcome variables (total average positive power; total average negative power; individual joint contributions to average positive and negative powers; net metabolic power, and efficiency) between hemiparetic and

control participants, an ANOVA with a Bonferroni adjustment was used. A post-hoc Tukey analysis was performed further distinguish significance between the independent variables for paretic, non-paretic, and control limbs. For all statistical tests, an α level of 0.05 was set as the threshold for significance.

Results

Our participants had a stroke at least six months prior to this study. They walked with an average preferred walking speed of $0.85 \pm 0.23 \text{ m s}^{-1}$ and were on average 58 ± 11 years of age. The non-disabled controls were on average 25 ± 5 years of age.

Average Mechanical Power Output

The participants produced significantly more total joint positive mechanical power with their combined limbs in comparison to the non-disabled controls, $0.67 \pm 0.13 \text{ W kg}^{-1}$ vs. $0.50 \pm 0.05 \text{ W kg}^{-1}$ (ANOVA: $p = 0.002$) (Appendix A Table 2, Appendix B Figure 3). The combined hemiparetic hip joints produced significantly more average positive power in comparison to the unimpaired hip joints, $0.32 \pm 0.09 \text{ W kg}^{-1}$ and $0.19 \pm 0.08 \text{ W kg}^{-1}$ respectively (ANOVA: $p = 0.005$).

The total limb positive power produced by the non-paretic leg ($0.43 \pm 0.09 \text{ W/kg}$) was significantly greater than the total control ($0.25 \pm 0.03 \text{ W/kg}$) and paretic ($0.24 \pm 0.07 \text{ W/kg}$) legs (ANOVA: $p < 0.0001$). When inspecting mechanical power production of the individual joints, the ankle joints and the hip joints showed significant differences among participants and between controls. The non-paretic ankle joint ($0.16 \pm 0.07 \text{ W/kg}$) performed

significantly more average positive power over the stride when compared to the paretic ankle joint (0.08 ± 0.04 W/kg). The power output by the non-paretic hip joint was significantly higher than the paretic and control hip joints, 0.21 ± 0.07 W/kg, 0.11 ± 0.04 W/kg, and 0.10 ± 0.04 W/kg, respectively (Appendix A Table 2).

Although the combined limbs absorbed similar amounts of total power, the hemiparetic ankle joints absorbed more negative power than the combined control limbs, -0.30 ± 0.06 W kg^{-1} vs. -0.22 ± 0.06 W kg^{-1} (ANOVA: $p = 0.04$). At the individual joints level, the non-paretic knee joint absorbed more negative power when compared to paretic, but was not different than control (-0.15 ± 0.03 W kg^{-1} , -0.11 ± 0.03 W kg^{-1} , 0.14 ± 0.03 W kg^{-1}) (ANOVA: $p = 0.04$).

Net Metabolic Power and Efficiency

Net metabolic power (W/kg) for the participants (3.2 ± 0.53 W/kg) was 51% higher when compared to the unimpaired controls during walking at 0.75 m s^{-1} (2.1 ± 0.72 W/kg) (ANOVA: $p = 0.003$) (Appendix B Figure 5).

The joint-level efficiency for hemiparetic walking ($\eta = 0.21 \pm 0.02$) was lower when compared to non-disabled controls ($\eta = 0.28 \pm 0.17$) walking at 0.75 m s^{-1} , but it was not significantly different.

Discussion

The aim of this study was to simultaneously examine joint mechanics and metabolic cost during post-stroke walking and draw comparisons to unimpaired controls at a fixed

speed. As expected from past studies^{4, 9, 14, 15}, the net metabolic power was 51% higher post-stroke when compared to their unimpaired counterparts walking at 0.75 m s^{-1} on a treadmill. We further hypothesized that the total positive average mechanical power across the joints for both limbs would be higher post-stroke when compared to unimpaired controls. In support of that hypothesis, the data from this study showed that the total average positive mechanical power summed across the joints of the lower limb was 37% higher (Appendix B Figure 3). Nearly all of the additional total average positive mechanical power post-stroke was produced by the unaffected limb. When compared to the control and paretic limbs, the non-paretic limb produced almost double the amount of positive mechanical power (0.43 W kg^{-1} vs. 0.24 W kg^{-1} and 0.25 W kg^{-1} respectively).

Unimpaired controls have been shown to produce approximately 40 % of the total limb positive power at the hip joint⁶, and we hypothesized the hip joint contribution post-stroke would increase due to compensations resulting from weak ankle push-off. Not only did the total joint average positive mechanical power increase post-stroke, but as we expected the hip joint contributed a higher percentage of the total work in comparison to non-disabled controls. This trend held for both paretic (39% vs. 47%) and non-paretic (39% vs. 49%) limbs as well as for the limbs combined (39% vs. 48%) (Appendix B Figure 3). This clearly demonstrates a higher level of reliance on the hip joint during walking post-stroke and is consistent with previous literature^{2, 3, 5}.

Finally, we hypothesized that the heavy reliance on the hip joint would limit the benefits of producing positive power at more compliant distal joints, e.g. ankle, and result in a lower

efficiency for the movement based on the lack of a large series elastic element in series with muscle. Although there was a trend toward lower joint-level efficiency post-stroke (0.21 vs. 0.28), the reduction was not significant. This finding is in line with previous reports based on center of mass (COM) mechanics calculations in which hemiparetic muscles performed at 0.20 efficiency⁴. Upon further examination, it is not that surprising that the overall efficiency is similar for hemiparetic versus control walking at 0.75 m s⁻¹. The apparent efficiency of hip joint muscle-tendon units at 1.25 m s⁻¹ walking speed has been estimated at ~0.24¹⁰, and that data can be extrapolated, using ankle joint apparent efficiency of 1.18 to yield hip joint apparent efficiency of 0.18 at 0.75 m s⁻¹. Our data indicated that when comparing unimpaired controls to the participants at 0.75 m s⁻¹ the net metabolic power increases by 0.9 W kg⁻¹ (from 2.1 to 3.2 W kg⁻¹) while the average positive mechanical power summed across the joints increased by 0.17 W kg⁻¹ for a delta efficiency of approximately of 0.19. The similarity between delta efficiency and hip joint apparent efficiency supports the idea that elevated metabolic cost of post-stroke walking can be accounted for solely by the additional work done by inefficient hip muscle-tendon units (paretic and non-paretic limbs).

It is worth noting that when applying apparent efficiencies estimated for ankle (1.18), knee (0.18), and hip (0.18)²¹ from unimpaired walking at 0.75 m s⁻¹ to post-stroke mechanics data we underestimate net metabolic power by 16%. This may indicate altered apparent efficiency of the knee and/or ankle muscle-tendon units post-stroke. We rule out major differences in hip apparent efficiency between participants and unimpaired subjects due to

the similarity between delta efficiency comparing populations and the previous reported apparent efficiency of the hip joint noted above.

Joint power outputs result from the product of angular velocities and moment at a given joint. Interestingly, our results indicate that deficits in the ankle joint power outputs in the paretic limb were due to similar deficits in both moment and angular velocity (Appendix B Figure 2). Therefore, not only do the ankle joint plantarflexors have reduced ability to produce appropriate forces but an increased joint stiffness¹³, may also limit ability to produce rapid movements and deliver sufficient mechanical power (Appendix B Figure 1)^{2-4, 13, 22}.

In order to improve efficiency and lower energy costs post-stroke, a rehabilitative program should focus on restoring paretic ankle joint strength, improving the already existing strength of the hip joints, and/or incorporating wearable robotic devices²³. In addition, our results support the contention by Cruz et al. that it may be beneficial to look into a multi-joint therapy regiment based on their findings that hip extensor strength is a crucial component in advancing a person's gait speed²⁴. Based upon the results in our study (Appendix B Figures 1-3), the paretic ankle joint consistently acts at a lower performance level which consequently results in decreased ability to produce adequate amounts of power local to that joint. If a therapist could implement strengthening regiments focusing on improving range of motion and muscle strength post-stroke, the amount of power able to be produce would likely increase and help restore symmetry to the gait pattern in participants. In addition, our results demonstrate large deficits in ankle angular velocities indicating that exercises targeting flexibility as well as muscle strength may fully serve the participants. Simultaneously

focusing on hip joint strength could add additional benefits for helping improve efficiency of hemiparetic walking. The increased strength of the hip joint would enable the musculature to bear larger loads and operate at a higher efficiency for a given walking speed. In some cases where symptoms post-stroke are irreversible, an actively or passively powered rehabilitative device can be used to help minimize asymmetry²⁵⁻²⁷. These devices could focus on compensating for the shortcomings of the paretic ankle joint in order to restore symmetry and/or directly power the hip joint to offload the added mechanical demand post-stroke.

It is worth noting a number of limitations in the current study. We were unable to carefully match size and age amongst controls and hemiparetic cohorts (Appendix A Table 1). This may lead to confounding influences of age and stature on our outcome variables. In addition, although the average overground walking speed of our participants ($0.85 \pm 0.23 \text{ m s}^{-1}$) was well below normal ($1.25 - 1.5 \text{ m s}^{-1}$) it was still on the high end for post-stroke walking (i.e. community ambulatory, relatively high-functioning). Future studies should address differences between participants across a larger range of function and aim to make comparisons with closely-matched unimpaired controls across a range of walking speeds. Finally, some of the assumptions inherent in inverse dynamics analyses regarding the co-activations amongst agonist and antagonistic muscle pairs as well as energy transfers amongst joints may be challenged in impaired populations. For example, in unimpaired walking antagonistic muscles have been shown to account for almost 7% of the actual musculo-tendon positive work and can result in inverse dynamics underestimates over the

lower-limb¹⁶. Antagonistic muscles may be relatively more active post-stroke. Future studies should implement an integrative approach including motion capture, force ergometry, electromyography (EMG), and perhaps *in vivo*²⁸ and model-based techniques²⁹ to address individual muscular behavior during dynamic walking post-stroke.

Finally, the age differences in our subjects could have led to confounding results. We showed the paretic ankle joint was weaker in the subjects who experienced a stroke when compared to the non-paretic ankle joint and the unimpaired controls, but the large age differential may have attributed to the variations in the gait kinetics and kinematics³⁰ as well as the after effects of a stroke. Rudolph et al. demonstrated a weakened muscle groups associated with aging³⁰. The weakness on the paretic side could have been attributed to the aging process, which was not considered in this study. In future studies, an age-matched control population would help eliminate age differences apparent in this study.

Conclusions

We analyzed the links between the redistribution of lower-limb joint positive mechanical power and the elevated metabolic expenditure post-stroke. We found that the total combined joint (ankle + knee + hip) positive mechanical power for both limbs in the participants was increased by 34% in comparison to the non-disabled control. As expected from previous work, the net metabolic power was also increased post-stroke by 51%. Our results suggest that much of the additional metabolic demand is due to added power output in the paretic and non-paretic hips. Surprisingly, despite no difference in total joint power-based efficiency between hemiparetic and control walkers at 0.75 m s^{-1} , increases in metabolic cost (51%)

were not proportional to increases in mechanical demand (34%). This may be explained by altered efficiency of the individual joints post-stroke when compared to unimpaired controls. For example, asymmetric ankle push-off may reflect underlying disruption of finely-tuned elastic energy storage and return in an effective catapult mechanism.

Medial Gastrocnemius Muscle Behavior During Post-Stroke Walking

Introduction

The ankle joint produces nearly half of the total joint mechanical power output in nondisabled gait^{6, 10}. Ankle joint mechanical power is primarily responsible for producing an efficient push-off that aids in forward propulsion. Furthermore, the plantarflexors (soleus, medial and lateral gastrocnemius) make up one of the most efficient musculotendon systems in the body^{6, 10, 28}. The triceps surae muscles (the contractile element CE) act in series with the long Achilles tendon (the series elastic element SEE) which serves as an effective energy storage and return mechanism. For example, recoil of the tendinous portion of the medial gastrocnemius (MG) muscle-tendon unit (MTU) delivers approximately half of the average positive mechanical power during late stance in both walking and running²⁸. In essence, the tendinous tissues act like a catapult mechanism by passively storing energy while being stretched during stance then injecting the system with that elastic energy via rapid recoil^{22, 31}. During tendon stretch, the MG fascicles remain relatively isometric, reducing their metabolic energy expenditure, owing to the fact that muscle uses more energy to do work than to produce force^{22, 31, 32}. If this finely tuned coordination between the SEE and CE is disturbed, the stored elastic energy may be dissipated and require additional mechanical work from fascicles at an increased metabolic cost.

There are a number of ways in which the tuning of the catapult mechanism could be disrupted. One possibility is that the material properties (e.g. elastic modulus) of the

tendinous tissues in the MG-MTU may be altered by disease state, exercise or normal aging, to name a few. For example, older adults have been shown to have more compliant tendinous tissues in comparison to young adults³³. As a result, in older adults the tendon was maintained at a significantly longer length and the fascicles at a significantly shorter length after the initial stretch during heel strike in comparison to young adults³³. More recently, studies have begun to investigate tissue property changes in neurologically-impaired populations, for example, post-stroke³⁴. Using a dynamometer and ultrasound imaging, Gao et al. showed that the muscle fascicles undergo substantial contractile property changes, i.e. shifts in force-length relationship. They conclude that these alterations may lead to joint-level changes, i.e. increased stiffness, muscle weakness, decreased range of motion, and impaired motor function³⁴. Unfortunately, this study did not evaluate the impact of the altered properties during functional tasks, such as walking.

Computer simulations provide an alternative approach to examine muscle-level dynamics during function tasks. Recently, a forward modeling simulation study provided an ‘under the skin’ look at the muscle-tendon interaction mechanics²⁹. Peterson et al. found that the total positive work across the muscles of the lower limb (paretic + non-paretic) was increased post-stroke while the total positive tendon work was reduced²⁹. This is an indirect indication that participants may not be fully exploiting elastic tissues during gait. Though these models provide a powerful tool to investigate muscle-level questions, their predictions could be validated with experimental evidence from direct *in vivo* measurements, i.e. ultrasound imaging.

On the experimental side, previous studies using inverse dynamics analysis of hemiparetic walking have revealed weakened ankle plantar flexors on the paretic side^{2-5, 12, 13}. The resulting asymmetric ankle push-off likely leads to increase collisional losses⁷ requiring additional mechanical and metabolic energy for hemiparetic walking compared to unimpaired controls^{4, 5, 8, 9, 14, 15}. Unfortunately, these studies only examined the joint-level mechanics and due to limitation in measurement capabilities could not address potential differences in contributions of the musculature (CE) versus elastic tissues (SEE) of individual muscle-tendon units.

The aim of this study was to combine an inverse dynamics analysis with real-time ultrasound images to elucidate the differences in medial gastrocnemius fascicle length-change patterns post-stroke when compared to controls at a fixed gait speed.

We hypothesized that during walking at 0.75 m s^{-1} , compared to the non-disabled control MG, 1) the paretic MG muscle fascicles would undergo additional length changes due to decreased peak ankle joint moments and impaired force production, and 2) the non-paretic MG muscle fascicles would maintain ‘catapult-like’ isometric tuning within the muscle-tendon unit (MTU). Finally, owing to additional length changes in the paretic MG fascicles, we expected the total average positive power of the combined (paretic + non-paretic) MGs to be higher post-stroke.

Materials and Methods

Experimental Protocol

Eight walkers who had a stroke (participants) and did not use an ankle-foot orthotic (AFO) (mean \pm s.d., age = 58 ± 11 years ; mass = 95 ± 19 kg; height = 1.77 ± 0.06 m) and nine unimpaired controls (controls) (mean \pm s.d, age = 25 ± 5 years; mass = 72 ± 13 kg; height = 1.69 ± 0.16 m) provided us with an institutional review board (IRB) approved consent form to participate in this study. A more in depth listing of subject characteristics is outlined in Appendix A Table 1. All procedures were approved by the University of North Carolina, Chapel Hill and North Carolina State University institutional review boards (IRB) and followed the procedures outlined by the Declaration of Helsinki.

All trials were completed on an instrumented treadmill (BERTEC, Columbus, OH, USA) set to 0.75 m s^{-1} and lasted four minutes. Each participant wore a harness to reduce the possibility for falls or injury. The harness did not supply any body weight support. The participants were discouraged from using the handrails other than for small balance corrections throughout the trials

Kinetics and Kinematics

An eight camera motion analysis system (VICON, Oxford, UK) was used to capture the position of 37 reflective markers attached to the pelvis, right leg, and left leg (modified Cleveland Clinic marker set) at 120 Hertz. Raw marker positions were filtered using a second-order low pass Butterworth filter with a cut-off frequency of 10 Hertz. A static standing trial was captured and the positions of the markers on segment endpoints were used

to calibrate a four segment (comprised of one pelvis, two thighs, two shanks, and two feet) model on both legs for each subject using established inertial parameter¹⁷. Clusters of three to four markers on rigid plates were attached to the pelvis, thigh, and shank segment to track segment motion on both the left and right leg during the trials. For the foot, a cluster of three markers was attached directly to the walker's shoe. Joint angle for the hip, knee, and ankle were computed in three dimensions as the orientation of the distal segment with reference to the proximal segment and differentiated to calculate joint velocities.

The force data was recorded at 120 Hertz during the movement trial at 0.75 m s^{-1} using two force platforms underneath each belt of the instrumented. The subjects were allowed to choose their step frequency and length freely, were allowed to grip the handrail while the treadmill reached the prescribed speed, and were asked to release the handrail once the speed was obtained. Each participant was required to walk with each foot hitting its ipsilateral treadmill belt and force platform to ensure that individual limb was contributing to that leg's calculations in the double support phase of the gait cycle. The raw force analog data were filtered with a second-order low-pass Butterworth filter with a cut-off frequency of 35 Hertz. Inverse dynamic analyses¹⁸ were then used to compute net joint moments, which were multiplied by the calculated joint angular velocities to calculate joint powers for the hip, knee, and ankle joints. Kinematics and kinetics were calculated for the left and the right leg individually for the participants, but for the unimpaired controls symmetry was assumed and the kinetics and kinematics were calculated for the right leg. The calculations of kinetics and

kinematics were performed using a combination of Visual 3-D software (C-Motion Inc., Germantown, MD, USA) and MATLAB (MathWorks, Natick, MA, USA).

Determination of Gastrocnemius Muscle Length Change Patterns

The length-change pattern of the medial gastrocnemius muscle fascicles were measured during the 0.75 m s^{-1} trial using a B-mode ultrasound probe to collect real-time images³⁵. A linear ultrasound transducer (LV7.5/60/96Z; Telemed) operating at 8.0 MHz was placed over the muscle belly of the medial gastrocnemius and aligned so that the muscle fascicles could be visualized from deep to superficial aponeurosis (Appendix B Figure 6). Images were sampled at 50 Hz, and a pulse from the ultrasound system that was high (3-5V) during recording and low (0 V) before and after was used to trigger the collection of the data simultaneously. A custom MATLAB (MathWorks) program was written to obtain the fascicle length-change pattern. Two different points were chosen during the digitization of the image, the deep and the superficial aponeuroses, and the distance between of the two points was determined to be the length of the fascicle. The pennation angle θ of the muscle fascicle was defined as the angle between the digitized fascicle and the superficial aponeurosis (Appendix B Figure 6). The instantaneous length of the whole medial gastrocnemius muscle-tendon unit was calculated from the ankle and knee joint angle using the equations of Hawkins and Hull³⁶. The length of the series elastic element (SEE) was found by multiplying the length of the muscle fascicle by the cosine of the pennation angle θ and subtracted from the MTU length³⁵ (Appendix B Figure 6). This approach neglects any angle between the aponeurosis and external tendon of the medial gastrocnemius and could

result in slight underestimation of the SEE length. The initial muscle fascicle length (L) was recorded at heel strike, and the fascicle length change (ΔL) was calculated relative to L .

Calculation of the Gastrocnemius Muscle Kinetics

Muscle and tendon forces were unable to be directly measured *in vivo*. The inverse dynamics and measured muscle parameters were used to estimate the muscle and tendon kinetics and kinematics. The force in the Achilles tendon (AT) was calculated as the net ankle flexion-extension moment divided by the moment arm of the AT in accordance to previous method^{37, 38}. The instantaneous moment arm of the AT was calculated as the first derivative of the MG MTU length with respect to ankle angle^{39, 40}. The force contribution by the MG was estimated by multiplying the AT force by the relative PCSA of the MG within the plantar-flexors⁴¹, which was taken as 0.159 (equation 1 in ref. ⁴²). This force was considered the force in the SEE of the MG. To estimate the force in the muscle fascicles, the force in the SEE was divided by the cosine of the MG pennation angle (equation 2 in ⁴³). This approach to calculate muscle force does not account for any contribution of antagonistic dorsiflexors to the net ankle moment, although this was assumed not to be significant during stance phase. This was when the tibialis anterior is minimally inactive⁴⁴. This PCSA-based approach also assumes similar relative activations among plantar flexors during the trial.

The velocities of the MG fascicles, MTU and SEE were calculated as the first derivative of their lengths with respect to time. The power output of the fascicles, SEE, and MTU were then calculated as the product of respective forces and velocities (equations 3-5). Positive work done by the fascicles, SEE and, MTU were estimated by integrating the positive

portions of each component's power curve. Periods of positive power during the trial were integrated using the trapezium method, summed, and then divided by the number of strides taken to calculate average positive work done per stride. This same approach was done for the negative work calculations except the negative portions of the power curve were integrated using the trapezium method. These values were divided by stride time to convert to average power for fascicle, CE $\left(\overline{P_{CE}^{\pm}}\right)$, tendinous tissues, SEE $\left(\overline{P_{SEE}^{\pm}}\right)$, and whole muscle-tendon unit, MTU $\left(\overline{P_{MTU}^{\pm}}\right)$. The ideal (most efficient) scenario would be for the fascicle power $\left(\overline{P_{CE}^{\pm}}\right)$ to be zero (fascicle remains isometric) with all power $\left(\overline{P_{MTU}^{\pm}}\right)$ supplied by the SEE $\left(\overline{P_{SEE}^{\pm}}\right)$, i.e. tuned. In equation 1, F_{SEE} is the force due to the medial head of the medial gastrocnemius, F_{AT} is the force due to all plantar flexors, and 0.159 is the relative physiological cross-section of the MG within the plantar flexors (compared to 0.57 for the soleus, 0.065 for the lateral gastrocnemius, and the remainder due to other plantar flexors). In equation 2, F_{CE} is the force in the muscle fascicle and θ is the pennation angle (in radians). In equation 3, P_{MTU} is the MTU power and V_{MTU} is MG MTU velocity. In equation 4, P_{SEE} is the SEE power and V_{SEE} is the SEE velocity. In equation 5, P_{CE} is the MG fascicle power and V_{CE} is the MG fascicle velocity.

$$F_{SEE} = F_{AT} \cdot 0.159 \quad (1)$$

$$F_{CE} = F_{SEE} \cdot (\cos \theta)^{-1} \quad (2)$$

$$P_{MTU} = F_{SEE} \cdot V_{MTU} \quad (3)$$

$$P_{SEE} = F_{SEE} \cdot V_{SEE} \quad (4)$$

$$P_{CE} = F_{MG} \cdot V_{CE} \quad (5)$$

The key outcome variables identified at 0.75 m s⁻¹ were the maximum force produced by the fascicles (F_{MGmax}); the percent of the stride when maximum fascicle force occurs; the velocity of the CE (V_{CE}), SEE (V_{SEE}), and MTU (V_{MTU}) at the time of maximum fascicle force; the length change of the CE (ΔL_{CE}), SEE (ΔL_{SEE}), and MTU (ΔL_{MTU}) at the maximum fascicle force; and the average positive and negative mechanical power outputs for the MTU and its elements $\overline{P_{CE}^{\pm}}$; $\overline{P_{SEE}^{\pm}}$; $\overline{P_{MTU}^{\pm}}$.

Statistical Analysis

For each individual, kinematic and kinetic data were averaged over 8-10 strides. Group means and standard deviations were then computed and, unless otherwise stated, these values are the values represented in the text. To test for differences in outcome variables listed above between conditions (paretic, non-paretic and control), an ANOVA with a Bonferroni adjustment was used. We used Tukey post-hoc tests was performed to make pair-wise comparisons between the paretic, non-paretic, and control limbs for significant variables. For all statistical tests, an α level of 0.05 was set as the threshold for significance.

Results

Our participants had a stroke at least six months prior to this study. They walked with an average preferred walking speed of 0.85 ± 0.23 m s⁻¹ and were on average 58 ± 11 years of age. The non-disabled controls were on average 25 ± 5 years of age.

Ankle Powers, Moments, and Angular Velocities

The non-paretic peak ankle power (Appendix B Figure 7) was significantly higher than the paretic peak ankle power (1.89 W kg^{-1} vs. 0.77 W kg^{-1}) while walking at 0.75 m s^{-1} (ANOVA: $p = 0.002$), but neither were different from controls. Differences in peak plantarflexor moment (-1.07 Nm kg^{-1} vs. -1.30 Nm kg^{-1}) (ANOVA: $p = 0.02$) and peak plantar flexor angular velocity (ANOVA: $p = 0.005$) contributed to the observed differences in power production between the paretic and non-paretic ankle joint.

Muscle Mechanics

In the non-disabled controls walking at 0.75 m s^{-1} , the MG MTU underwent a classic stretch-shortening cycle through the first 70% of the gait cycle (Appendix B Figure 8). The majority of the non-disabled MG MTU length-change was taken up by stretch and recoil of the SEE, while the CE remained relatively isometric.

The control MTU exhibited more shortening near the end of stance in comparison to the paretic and non-paretic MG MTU. In the CE behaviors, the control, paretic and non-paretic fascicles remained relatively isometric up until 40% of the gait cycle. Then, the non-paretic CE lengthened while the control CE began to shorten and the paretic CE maintained isometric behavior (Appendix B Figure 9). The control and non-paretic SEE experienced a larger range of motion in comparison to the paretic SEE. There was also less recoil in the paretic SEE late in the gait cycle.

Despite these qualitative differences in length-change patterns within the muscle-tendon unit, we found few significant differences when comparing between the control, paretic, and

non-paretic MG. The only significant difference seen in the length-change pattern was that the non-paretic CE lengthened significantly more in comparison to the control CE at the time of peak muscle fascicle force (F_{MGmax}), -3.0 mm vs. 2.2 mm (ANOVA: $p = 0.04$), respectively (Appendix A Table 4).

Forces in paretic and non-paretic MG remained higher throughout stance and reached peak values earlier in stride when compared to the control MG (52% - C, 47% - NP and 48% - P). We did not find any significant differences in the force production of the MTU, CE and the SEE across the three limbs (non-paretic = 294 ± 100 N; paretic = 263 ± 99 N; control = 260 ± 87 N).

The MG MTU peak in magnitude of power occurred after the time of peak force (~60% of stride) and trended higher in the control MG MTU (19 ± 5 W) in comparison to the paretic (15 ± 16 W) and non-paretic (17 ± 18) MG MTUs. Differences in peak power output were due to differences in peak shortening velocities for the MG MTUs and the controls (83.35 ± 30 mm s⁻¹) had higher magnitudes in the peak power output in comparison to the paretic (53.38 ± 21 mm s⁻¹) and non-paretic (63.6 ± 17 mm s⁻¹) MG MTUs. There were no differences in MG MTU velocities at the time of maximum force (ANOVA: $p = 0.13$) (Appendix A Table 4). Although there were deviations in positive peak power production in the MG MTU, neither the average positive or negative mechanical power output of the MG MTU were significantly different between limbs (Appendix A Table 3 and Appendix B Figure 11).

The MG fascicles maintained low magnitude velocities (less than 50 mm s^{-1}) for paretic, non-paretic and control limbs through stance indicating relatively high level of isometry, even post-stroke. Though MG CE velocities did not largely fluctuate, the combination of slightly higher force and significant lengthening velocity beginning at approximately 30% of the gait cycle resulted in both non-paretic ($-2.09 \pm 0.78 \text{ W}$) and paretic ($-2.06 \pm 0.62 \text{ W}$) MG CEs absorbing significant amounts of mechanical energy when compared to control ($-0.67 \pm 0.64 \text{ W}$) (ANOVA: $p = 0.0002$) (Appendix A Table 3 and Appendix B Figure 10).

The MG SEE forces and velocities behaved similarly to the MG MTU indicating a large amount of decoupling between the fascicles and whole MTU due to significant compliance in the MG MTU. Up until 40% of the stride, the control, paretic, and non-paretic MG SEEs store significant amounts of strain energy. The control and paretic limbs continue to store elastic energy until about 50% of the stride while the non-paretic MG SEE begins to recoil much earlier (Appendix B Figure 10). Despite these differences in timing of recoil, the average MG SEE mechanical power output did not differ across limbs (Appendix A Table).

There were no significant differences in relative contributions of MG CE versus MG SEE to total average positive mechanical power output with all limbs roughly following 40% CE and 60% SEE (Appendix B Figure 11). The control MG MTU (80%) absorbed a much larger portion of average mechanical power in the SEE in comparison to paretic (52%) and non-paretic (51%) SEEs (ANOVA: $p < 0.0001$).

Discussion

In this study, we compared the muscle-tendon interaction mechanics within the medial gastrocnemius muscle-tendon unit during walking between hemiparetic and unimpaired control participants. We used a novel combination of inverse dynamics calculations and real-time ultrasound images following the approach of Farris et al²⁸, which allowed us to independently address the mechanics of the whole MTU as well as its component CE and SEE.

We hypothesized that the behavior of the MG muscle fascicles (i.e. CE) in the paretic limb would be altered as a result of the inability to produce adequate plantarflexor forces/moments at the ankle. Our data did not support this contention. Though the peak ankle moments for the paretic limbs were approximately 14% lower in the paretic limb in comparison to the control and non-paretic limbs (Appendix B Figure 7), the forces produced by the MTU, CE, and SEE were comparable among the limbs (Appendix B Figure 10). This disconnect is likely due to differences in posture (i.e. ankle joint angles) that may impact the moment arm of the MG MTU throughout the stride. As a result of undiminished force generation compared to controls, the paretic MG fascicle length-change behavior was not altered. This was indicated by no difference in length-change of the CE at the time of maximum force between paretic and control limbs (Appendix A Table 4 and Appendix B Figure 8-9). It is worth noting that the behavior may not hold for faster walking speeds where demand for force is likely increased. However, in that case it may still be possible to maintain isometric fascicles if there are accompanying adaptations in the material properties

within the MTU³⁴. For example, increased compliance of the SEE could allow for the CE to operate at more favorable lengths for force production in order to maintain isometric tuning³³.

In contrast to the paretic MG, we expected that intact force production capability in the non-paretic MG muscle fascicles would maintain isometric tuning and a functional catapult mechanism similar to the control MG. Although as expected the peak forces were no different than controls, to our surprise the non-paretic muscle fascicles exhibited 173% more lengthening in comparison to unimpaired controls at the time of the maximum force production (Appendix A Table 4 and Appendix B Figures 9-10). A likely factor behind this finding is that mistimed and asymmetric propulsion mechanics inherent in post-stroke walking cause more violent collisions, especially in the non-paretic leading limb. These collisions require additional energy dissipation as indicated by large amounts of energy absorption (i.e. negative power outputs) during stance in the non-paretic ankle joint and MG MTU (Appendix B Figure 7 and 10). The non-paretic MG muscle fascicles undergo significantly more lengthening and absorb large amounts of mechanical power (~2 W) between 30 and 50% of the stride. Interestingly, paretic MG fascicles absorb similar amounts of mechanical energy (~2 W). Rather than recycling additional energy in elastic tissues, both paretic and non-paretic limbs dissipate energy in the MG fascicles (Appendix B Figure 11). This is especially notable in the non-paretic MG where energy absorbed by fascicles results in a shorter period of energy storage in the elastic tissues as compared to paretic and control

MG (Appendix B Figure 10). As such, fascicle energy occurs simultaneous with SEE recoil (~40-50% of stride) resulting in ‘backfire’ of energy in the non-paretic MTU.

Our data indicated no significant increase in the overall positive fascicle work done by the paretic + non-paretic MG in comparison to the combined (left + right) control MG fascicles. To our surprise, the muscle-tendon interaction in the paretic MG was similar to controls, and although there were changes in the non-paretic muscle-tendon interaction (i.e. additional fascicle lengthening), they tended to increase negative rather than positive fascicle work. A computer simulation study by Peterson et al. concluded that during the period of pre-swing the total (paretic + non-paretic) net fiber work across the lower limb was higher during hemiparetic vs. unimpaired walking²⁹. Although our data for MG indicate no differences in paretic + non-paretic versus controls for average positive power of the MG CE, there was an increase negative work post-stroke. This is consistent with Peterson’s data for the gastrocnemius muscle during simulated walking indicating a decrease in net work of the gastrocnemius pre-swing in the paretic limb²⁹.

Interestingly, the manner in which positive mechanical power is partitioned across the components of the MG MTU (40% CE and 60% contributions) post-stroke did not deviate from unimpaired walkers at 0.75 m s^{-1} . This suggests that the ankle joint apparent efficiency should remain relatively high post-stroke and comparable to intact walkers. Based on Sawicki et al., at 0.75 m s^{-1} every 1 Joule of ankle joint mechanical work would require 0.85 J of metabolic energy (apparent efficiency equals 1.18)²¹. Therefore, elevations in metabolic

energy consumption post-stroke are likely dominated additional mechanical work performed by proximal muscle-tendon units (i.e. hip).

Our future research will aim to extend our *in vivo* approach in order to study other plantarflexors (i.e. soleus) and evaluate their neuromechanical performance. This is important because mechanical power production could be shifted to other muscles acting at the ankle or other joints post-stroke³. Furthermore, combining measurements of muscle activation (e.g. electromyography EMG) with muscle-level mechanics measurements (i.e. ultrasound imaging) may further improve our understanding of the consequences of disrupted reflexes post-stroke. For example, it is clear that motor synergies and interactions of stretch reflexes in hip and knee muscles are disrupted post-stroke⁴⁵⁻⁴⁷. However, clear links between altered muscle length-change patterns and muscle stretch reflexes remain elusive. This issue is particularly pressing for muscle with long series tendons where joint-level excursions are not necessarily representative of underlying fascicle length changes⁴⁸.

It's worth noting limitations with both our experimental and musculoskeletal modeling approaches to studying muscle-tendon interaction in impaired populations, such as stroke. Future studies should attempt to characterize these changes for more muscles of the lower limb (e.g. Gao et al³⁴) and integrate them into model predictions. Similarly, our *in vivo* approach extends assumptions used in non-disabled populations that may not hold post-stroke. For example, we assumed the amount of force produced by the medial gastrocnemius muscle is approximately 15% of the total force of the ankle extensors based on past research

documenting relative contributions to total cross-sectional area of the triceps surae muscle group⁴². Heterogeneous muscle atrophy may challenge this assumption post-stroke.

One major limitation is the age for the participants (58 ± 11 years) and the unimpaired controls (25 ± 5 years). It has been shown muscle strength decreases typically with age^{33, 49}, which could have majorly affected our results, but the non-paretic average positive power outputs for the CE values were comparable to the controls (Appendix A Table 3 and Appendix B Figure 11). This indicates the muscles in the participants were able to produce the adequate forces and were not subject to major muscular atrophy. Future studies will have age-matched controls with the participants to minimize any age-related effects.

Overall Conclusions and Future Directions

Because a stroke is such a debilitating disease that affects a large number of people, researchers have been diligently working to understand the joint mechanics, muscle mechanics, and metabolic energetics underlying post-stroke walking. The main goals of these investigations was to improve our basic understanding of hemiparetic gait in order to help design rehabilitation regimes or better assistive devices capable of restoring mobility and quality of life for people who have survived a stroke.

The goals of these studies were: 1) to link joint mechanics with metabolic energy consumption and better understand the mechanisms behind elevated energy consumption post-stroke and 2) to perform an *in vivo* investigation in order to examine potential alterations in muscle mechanics of one of the major muscles of the triceps surae, i.e. medial gastrocnemius muscle.

We found that the total average summed positive power output from the combined lower-limb joints during hemiparetic walking was 37% higher in comparison to the non-disabled walking. We also found that the non-paretic limb did nearly double the amount of mechanical work when compared to the paretic and control limbs, demonstrating a severe asymmetry in power production. In order to compensate, the hip joint positive power production increased in both the paretic and non-paretic limbs by 60% when compared to combined unimpaired hip joints. Surprisingly, this did not result in a lower mechanical efficiency post-stroke because the hip joint efficiency is similar to the overall efficiency of walking at 0.75 m s^{-1} .

At the muscle-level, we found that the medial gastrocnemius muscle-tendon unit maintains a relatively tuned catapult mechanism through the majority of stance phase in both paretic and non-paretic limbs when compared to controls. A notable exception was in late stance when both paretic and non-paretic MG muscle fascicles absorbed considerable amounts of mechanical energy. Despite differences in the absorption (i.e. average negative power production), the portion of average positive power muscle versus tendon was not altered compared to controls (60% tendon and 40% fascicles). As such, the ankle joint apparent efficiency is likely not altered post-stroke.

Future studies could analyze other muscle groups post-stroke to determine how their behaviors are altered post-stroke. This work could bring insight to therapists and engineers alike and could help with the rehabilitation outcomes for people who have had a stroke. In

particular, our joint and muscle level approaches provide a powerful tool for determining which joint/muscles should receive focus in a given individual. Furthermore, these results indicate that robotic devices design to improve paretic ankle joint push-off could significantly reduce metabolic demand of post-stroke walking by reversing compensations seen at proximal joints (e.g. hip).

References

1. Roger VL, Go AS, Lloyd-Jones DM, Benjamin EJ, Berry JD, Borden WB, Bravata DM, Dai S, Ford ES, Fox CS, Fullerton HJ, Gillespie C, Hailpern SM, Heit JA, Howard VJ, Kissela BM, Kittner SJ, Lackland DT, Lichtman JH, Lisabeth LD, Makuc DM, Marcus GM, Marelli A, Matchar DB, Moy CS, Mozaffarian D, Mussolino ME, Nichol G, Paynter NP, Soliman EZ, Sorlie PD, Sotoodehnia N, Turan TN, Virani SS, Wong ND, Woo D, Turner MB. Executive summary: Heart disease and stroke statistics--2012 update: A report from the american heart association. *Circulation*. 2012;125:188-197
2. Chen G, Patten C. Joint moment work during the stance-to-swing transition in hemiparetic subjects. *J Biomech*. 2008;41:877-883
3. Chen G, Patten C, Kothari DH, Zajac FE. Gait differences between individuals with post-stroke hemiparesis and non-disabled controls at matched speeds. *Gait Posture*. 2005;22:51-56
4. Detrembleur C, Dierick F, Stoquart G, Chantraine F, Lejeune T. Energy cost, mechanical work, and efficiency of hemiparetic walking. *Gait Posture*. 2003;18:47-55
5. Jonkers I, Delp S, Patten C. Capacity to increase walking speed is limited by impaired hip and ankle power generation in lower functioning persons post-stroke. *Gait Posture*. 2009;29:129-137
6. Farris DJ, Sawicki GS. The mechanics and energetics of human walking and running: A joint level perspective. *J R Soc Interface*. 2012;9:110-118
7. Kuo AD, Donelan JM, Ruina A. Energetic consequences of walking like an inverted pendulum: Step-to-step transitions. *Exerc Sport Sci Rev*. 2005;33:88-97
8. Olney SJ, Monga TN, Costigan PA. Mechanical energy of walking of stroke patients. *Arch Phys Med Rehabil*. 1986;67:92-98
9. Reisman DS, Rudolph KS, Farquhar WB. Influence of speed on walking economy poststroke. *Neurorehabil Neural Repair*. 2009;23:529-534
10. Sawicki GS, Lewis CL, Ferris DP. It pays to have a spring in your step. *Exerc Sport Sci Rev*. 2009;37:130-138
11. Sasaki K, Neptune RR. Individual muscle contributions to the axial knee joint contact force during normal walking. *J Biomech*. 2010;43:2780-2784

12. Allen JL, Kautz SA, Neptune RR. Step length asymmetry is representative of compensatory mechanisms used in post-stroke hemiparetic walking. *Gait Posture*. 2011;33:538-543
13. Lamontagne A, Malouin F, Richards CL, Dumas F. Mechanisms of disturbed motor control in ankle weakness during gait after stroke. *Gait Posture*. 2002;15:244-255
14. Waters RL, Mulroy S. The energy expenditure of normal and pathologic gait. *Gait Posture*. 1999;9:207-231
15. Zamparo P, Francescato MP, De Luca G, Lovati L, di Prampero PE. The energy cost of level walking in patients with hemiplegia. *Scand J Med Sci Sports*. 1995;5:348-352
16. Sasaki K, Neptune RR, Kautz SA. The relationships between muscle, external, internal and joint mechanical work during normal walking. *J Exp Biol*. 2009;212:738-744
17. Dempster WT. *Space requirements of the seated operator*. 1955.
18. Winter DA. *Biomechanics and motor control of human movement*. New York: Wiley; 1990.
19. Brockway JM. Derivation of formulae used to calculate energy expenditure in man. *Hum Nutr Clin Nutr*. 1987;41:463-471
20. Margaria R. *Biomechanics and energetics of muscular exercise*. Oxford: Clarendon Press; 1976.
21. Sawicki GS, Ferris DP. Powered ankle exoskeletons reveal the metabolic cost of plantar flexor mechanical work during walking with longer steps at constant step frequency. *J Exp Biol*. 2009;212:21-31
22. Ishikawa M, Komi PV, Grey MJ, Lepola V, Bruggemann GP. Muscle-tendon interaction and elastic energy usage in human walking. *J Appl Physiol*. 2005;99:603-608
23. Marchal-Crespo L, Reinkensmeyer DJ. Review of control strategies for robotic movement training after neurologic injury. *J Neuroeng Rehabil*. 2009;6:20
24. Cruz TH, Lewek MD, Dhaher YY. Biomechanical impairments and gait adaptations post-stroke: Multi-factorial associations. *J Biomech*. 2009;42:1673-1677

25. Wiggin MB, Sawicki GS, Collins SH. An exoskeleton using controlled energy storage and release to aid ankle propulsion. *IEEE Int Conf Rehabil Robot.* 2011;2011:5975342
26. Shorter KA, Kogler GF, Loth E, Durfee WK, Hsiao-Wecksler ET. A portable powered ankle-foot orthosis for rehabilitation. *J Rehabil Res Dev.* 2011;48:459-472
27. Hitt J, Oymagil AM, Sugar T, Hollander K, Boehler A, Fleeger J. Dynamically controlled ankle-foot orthosis (dco) with regenerative kinetics: Incrementally attaining user portability. *Ieee Int Conf Robot.* 2007:1541-1546
28. Farris DJ, Sawicki GS. Human medial gastrocnemius force-velocity behavior shifts with locomotion speed and gait. *Proc Natl Acad Sci U S A.* 2012;109:977-982
29. Peterson CL, Kautz SA, Neptune RR. Muscle work is increased in pre-swing during hemiparetic walking. *Clin Biomech (Bristol, Avon).* 2011;26:859-866
30. Rudolph KS, Schmitt LC, Lewek MD. Age-related changes in strength, joint laxity, and walking patterns: Are they related to knee osteoarthritis? *Phys Ther.* 2007;87:1422-1432
31. Fukunaga T, Kubo K, Kawakami Y, Fukashiro S, Kanehisa H, Maganaris CN. In vivo behaviour of human muscle tendon during walking. *Proc Biol Sci.* 2001;268:229-233
32. Lichtwark GA, Bougoulias K, Wilson AM. Muscle fascicle and series elastic element length changes along the length of the human gastrocnemius during walking and running. *J Biomech.* 2007;40:157-164
33. Mian OS, Thom JM, Ardigo LP, Minetti AE, Narici MV. Gastrocnemius muscle-tendon behaviour during walking in young and older adults. *Acta Physiol (Oxf).* 2007;189:57-65
34. Gao F, Zhang LQ. Altered contractile properties of the gastrocnemius muscle poststroke. *J Appl Physiol.* 2008;105:1802-1808
35. Fukunaga T, Ichinose Y, Ito M, Kawakami Y, Fukashiro S. Determination of fascicle length and pennation in a contracting human muscle in vivo. *J Appl Physiol.* 1997;82:354-358
36. Hawkins D, Hull ML. A method for determining lower extremity muscle-tendon lengths during flexion/extension movements. *J Biomech.* 1990;23:487-494

37. Lichtwark GA, Wilson AM. In vivo mechanical properties of the human achilles tendon during one-legged hopping. *J Exp Biol.* 2005;208:4715-4725
38. Farris DJ, Trewartha G, McGuigan MP. Could intra-tendinous hyperthermia during running explain chronic injury of the human achilles tendon? *J Biomech.* 2011;44:822-826
39. Lichtwark GA, Wilson AM. Optimal muscle fascicle length and tendon stiffness for maximising gastrocnemius efficiency during human walking and running. *J Theor Biol.* 2008;252:662-673
40. Bobbert MF, Huijing PA, van Ingen Schenau GJ. A model of the human triceps surae muscle-tendon complex applied to jumping. *J Biomech.* 1986;19:887-898
41. Kurokawa S, Fukunaga T, Nagano A, Fukashiro S. Interaction between fascicles and tendinous structures during counter movement jumping investigated in vivo. *J Appl Physiol.* 2003;95:2306-2314
42. Fukunaga T, Roy RR, Shellock FG, Hodgson JA, Day MK, Lee PL, Kwong-Fu H, Edgerton VR. Physiological cross-sectional area of human leg muscles based on magnetic resonance imaging. *J Orthop Res.* 1992;10:928-934
43. Lichtwark GA, Wilson AM. Interactions between the human gastrocnemius muscle and the achilles tendon during incline, level and decline locomotion. *J Exp Biol.* 2006;209:4379-4388
44. Hreljac A, Arata A, Ferber R, Mercer JA, Row BS. An electromyographical analysis of the role of dorsiflexors on the gait transition during human locomotion. *Journal of Applied Biomechanics.* 2001;17:287-296
45. Cruz TH, Dhaher YY. Impaired lower limb muscle synergies post-stroke. *Conf Proc IEEE Eng Med Biol Soc.* 2009;2009:3956-3959
46. Finley JM, Perreault EJ, Dhaher YY. Stretch reflex coupling between the hip and knee: Implications for impaired gait following stroke. *Exp Brain Res.* 2008;188:529-540
47. Lewek MD, Breslin R, Hlad L, Lanton A, St John J. Non-paretic quadriceps activity influences paretic quadriceps activity post-stroke. *Clin Neurophysiol.* 2010;121:1962-1967
48. Maas H, Lichtwark GA. Is muscle-tendon unit length a valid indicator for muscle spindle output ? *J Physiol-London.* 2009;587:13-14

49. Williams GN, Higgins MJ, Lewek MD. Aging skeletal muscle: Physiologic changes and the effects of training. *Phys Ther.* 2002;82:62-68

Appendices

Appendix A – Tables

Table 1: Listing of participant characteristics. For the ‘stride time asymmetry metric’ reported in the last column, a perfectly symmetric gait scores zero.

Patient	Age (years)	Mass (kg)	Height (meters)	Time since stroke (years)	Paretic Side	Preferred Over-ground speed (m s ⁻¹)	Asymmetry in Stance Time (%)	Stance Time Asymmetry ³ Metric (%)
1	54	90	1.73	28	Left	1.02	43/57	23
2	45	69	1.75	5	Left	0.52	41/59	31
3	49	80	1.71	4	Left	0.74	46/54	16
4	56	82	1.77	4	Right	1.15	49/51	5
5	67	119	1.79	10	Right	0.78	49/51	4
6	80	90	1.72	9	Right	0.62	41/59	27
7	56	106	1.74	1	Left	0.88	43/57	23
8	55	121	1.91	7	Right	1.10	44/56	21
Mean ± SD	58 ± 11	95 ± 19	1.77 ± 0.06	9 ± 8	N/A	0.85 ± 0.23	45/55 ± 3/3	19 ± 10
Control	25 ± 5	72 ± 13	1.69 ± 0.16	N/A	N/A	N/A	N/A	N/A

Average combined positive and negative power (W) for the CE and the SEE of the control, paretic and non-paretic limb. The red shows the CE power contributions, where as blue represents the SEE contributions. Statistical significance is noted by: * = paretic different than control; # = non-paretic is different than control ($p < 0.05$).

Table 2: Average positive and negative powers ($W \text{ kg}^{-1}$) for the hemiparetic and the non-disabled control participants. The table shows the individual joint and total leg contributions. The various symbols indicate the significant differences (*: paretic different than non-paretic, #: non-paretic different than the control).

	Control	Hemiparetic		p-value
		Paretic	Non-Paretic	
\bar{P}^+ _{ankle}	0.10 ± 0.04	0.08 ± 0.04	0.16 ± 0.07	0.02: *
\bar{P}^+ _{knee}	0.05 ± 0.02	0.05 ± 0.03	0.06 ± 0.04	0.37
\bar{P}^+ _{hip}	0.10 ± 0.04	0.11 ± 0.04	0.21 ± 0.07	0.0003: *,#
Σ^+ _{joints}	0.25 ± 0.03	0.24 ± 0.07	0.43 ± 0.09	$p < 0.0001$: *,#
\bar{P}^- _{ankle}	-0.11 ± 0.03	-0.15 ± 0.03	-0.15 ± 0.05	0.13
\bar{P}^- _{knee}	-0.14 ± 0.03	-0.11 ± 0.03	-0.15 ± 0.03	0.04: *
\bar{P}^- _{hip}	-0.04 ± 0.03	-0.05 ± 0.03	-0.04 ± 0.03	0.65
Σ^- _{joints}	-0.29 ± 0.05	-0.31 ± 0.07	-0.34 ± 0.10	0.44

Table 3: Average positive and negative powers (W) for the control, paretic, and non-paretic MTU, CE, and SEE. The various symbols indicate the significant differences (*: paretic different than non-paretic, #: non-paretic different than the control).

	Control	Hemiparetic		p-value
		Paretic	Non-Paretic	
\bar{P}^+ _{MTU}	2.11 ± 0.66	1.65 ± 0.70	1.73 ± 0.94	0.43
\bar{P}^+ _{CE}	1.38 ± 0.81	1.34 ± 0.63	1.44 ± 0.97	0.97
\bar{P}^+ _{SEE}	2.10 ± 1.04	1.88 ± 0.68	2.55 ± 0.77	0.29
Σ^+ _{SEE+CE}	3.48 ± 1.64	3.22 ± 1.18	3.99 ± 1.51	0.57
\bar{P}^- _{MTU}	-1.59 ± 0.74	-1.29 ± 0.71	-1.95 ± 0.79	0.32
\bar{P}^- _{CE}	-0.67 ± 0.64	-2.05 ± 0.62	-2.09 ± 0.78	0.0002: *,#
\bar{P}^- _{SEE}	-2.29 ± 1.19	-2.25 ± 0.66	-2.36 ± 1.41	0.99
Σ^- _{SEE+CE}	-2.97 ± 1.61	-4.43 ± 1.23	-4.45 ± 2.16	0.14

Table 4: Maximum force of the MG muscle fascicles (N) for the control, paretic, and non-paretic limbs. Also the percent stride (%), the change in length (mm) and velocity (mm s^{-1}) of the MTU, CE, and SEE all recorded at the point in time of the gait cycle of the maximum force (@ Fmax). The significance between control and non-paretic MG is indicated with #.

	Control	Hemiparetic		p-value
		Paretic	Non-Paretic	
Max Force (N)	260.2 ± 87.3	263.84 ± 98.6	294.1 ± 100.2	0.73
% Stride_{@Fmax}	52 ± 3	48 ± 4	47 ± 4	0.05
$\Delta L_{\text{MTU@Fmax}}$ (mm)	9.3 ± 3.0	13.3 ± 4.8	14.9 ± 6.4	0.07
$\Delta L_{\text{CE@Fmax}}$ (mm)	-3.0 ± 3.6	-0.2 ± 2.7	2.2 ± 5.3	0.04: #
$\Delta L_{\text{SEE@Fmax}}$ (mm)	12.6 ± 3.5	13.0 ± 5.7	12.4 ± 9.1	0.98
$\vec{V}_{\text{MTU@Fmax}}$ (mm s^{-1})	1.8 ± 11.6	13.2 ± 9.1	12.1 ± 15.7	0.13
$\vec{V}_{\text{CE@Fmax}}$ (mm s^{-1})	-5.9 ± 23.8	0.2 ± 11.5	18.7 ± 36.2	0.15
$\vec{V}_{\text{SEE@Fmax}}$ (mm s^{-1})	6.7 ± 27.1	13.7 ± 11.6	-8.8 ± 35.0	0.24

Appendix B – Figures

Figure 1: Mean lower-limb joint angles (degrees) for post-stroke hemiparetic and neurologically intact control participants during walking at 0.75 m/s. Ankle (top panel), knee (middle panel) and hip (bottom panel) joint angles are plotted over a stride from heel strike (0%) to heel strike (100%) of the same limb. The solid black line represents the paretic limb, the dashed black line represents the non-paretic limb, and the gray line represents the control limb.

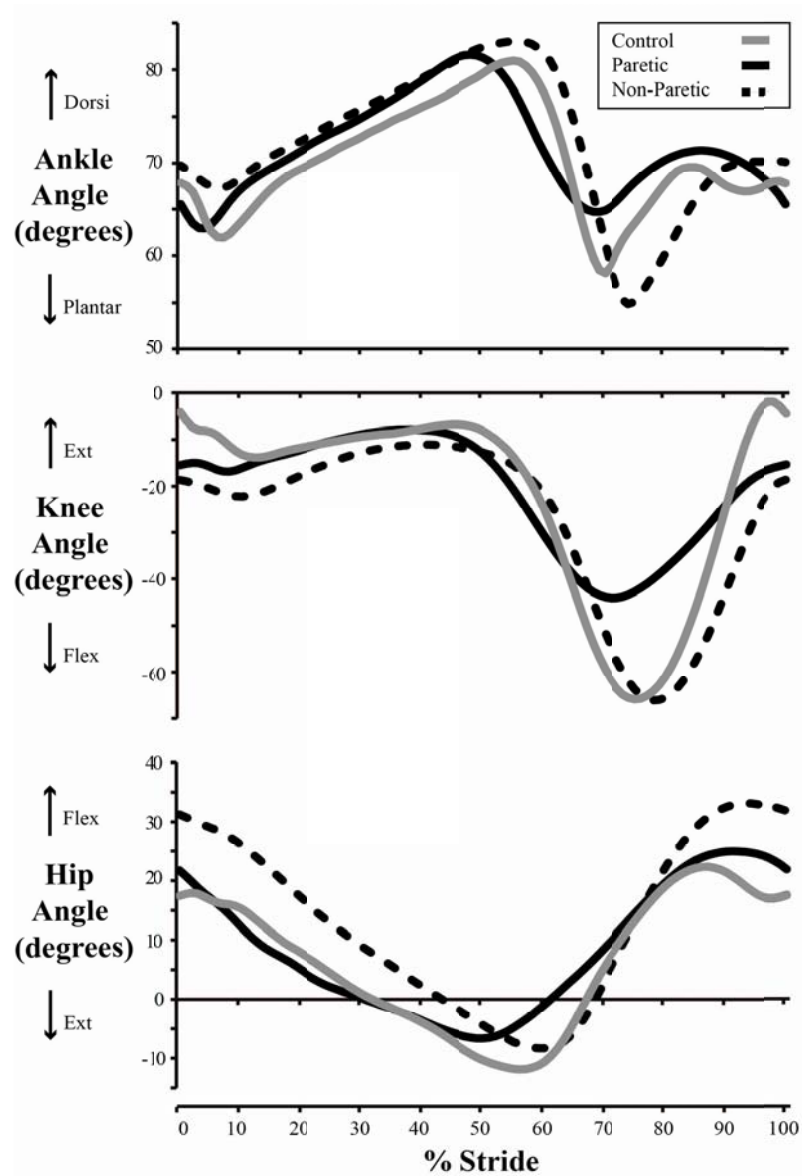


Figure 2: Ankle, knee and hip moment (N m^{-1}), angular velocity (degrees s^{-1}), and power (W kg^{-1}). The solid black line represents the paretic limb, the dashed black line represents the non-paretic limb, and the gray line represents the control limb.

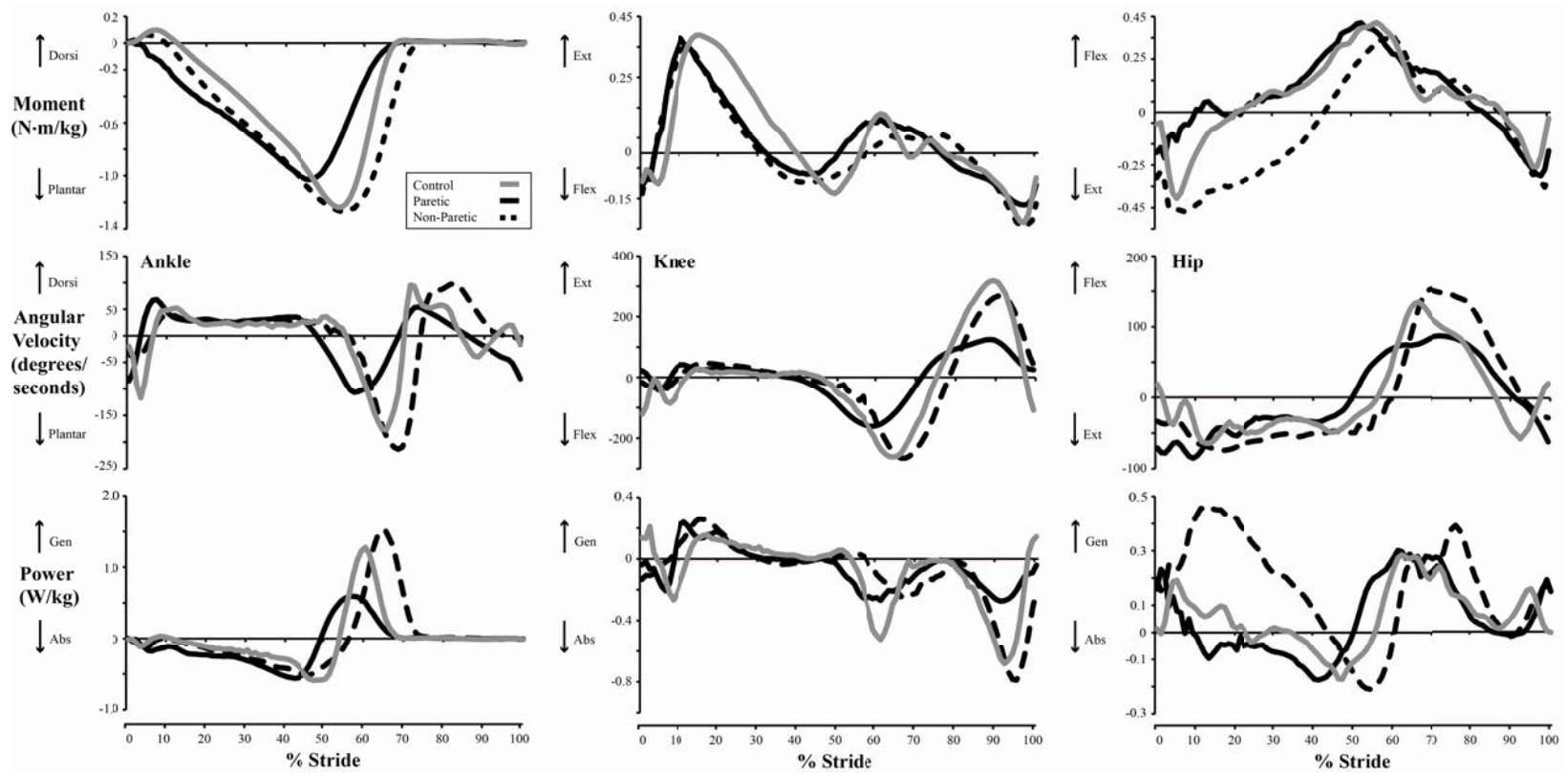


Figure 3: Total average positive power production for post-stroke hemiparetic and unimpaired control participants during walking at 0.75 m s^{-1} . The large pies represent the combined limb contributions to the total average positive mechanical power (W kg^{-1}) and are further broken down into each individual limb (two smaller pies below). Each pie is broken down into the different joints of the lower limb (ankle = black, gray = knee, and white = hip). The diameter of the pies is scaled to indicate the magnitude of positive power produced by that limb.

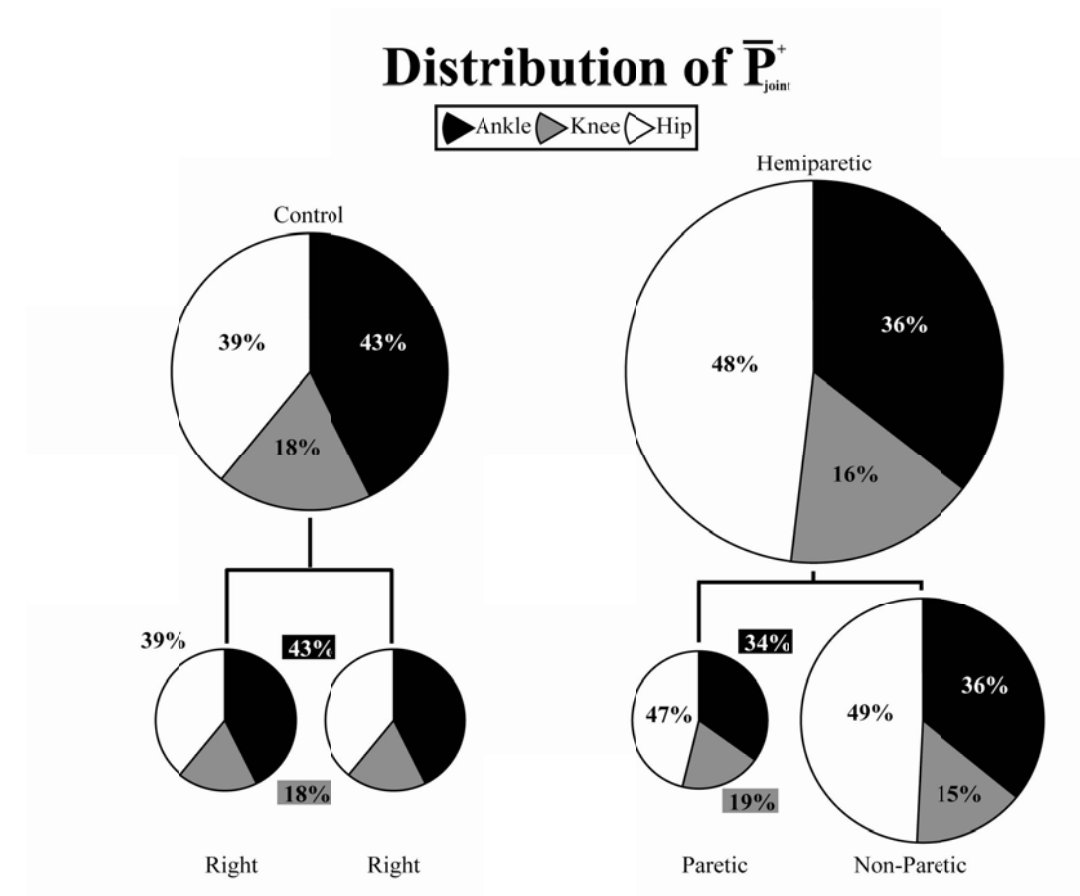


Figure 4: Total average negative power production for post-stroke hemiparetic and unimpaired control participants during walking at 0.75 m s^{-1} . The large pies represent the combined limb contributions to the total average positive mechanical power (W kg^{-1}) and are further broken down into each individual limb (two smaller pies below). Each pie is broken down into the different joints of the lower limb (ankle = black, gray = knee, and white = hip). The diameter of the pies is scaled to indicate the magnitude of negative power produced by that limb.

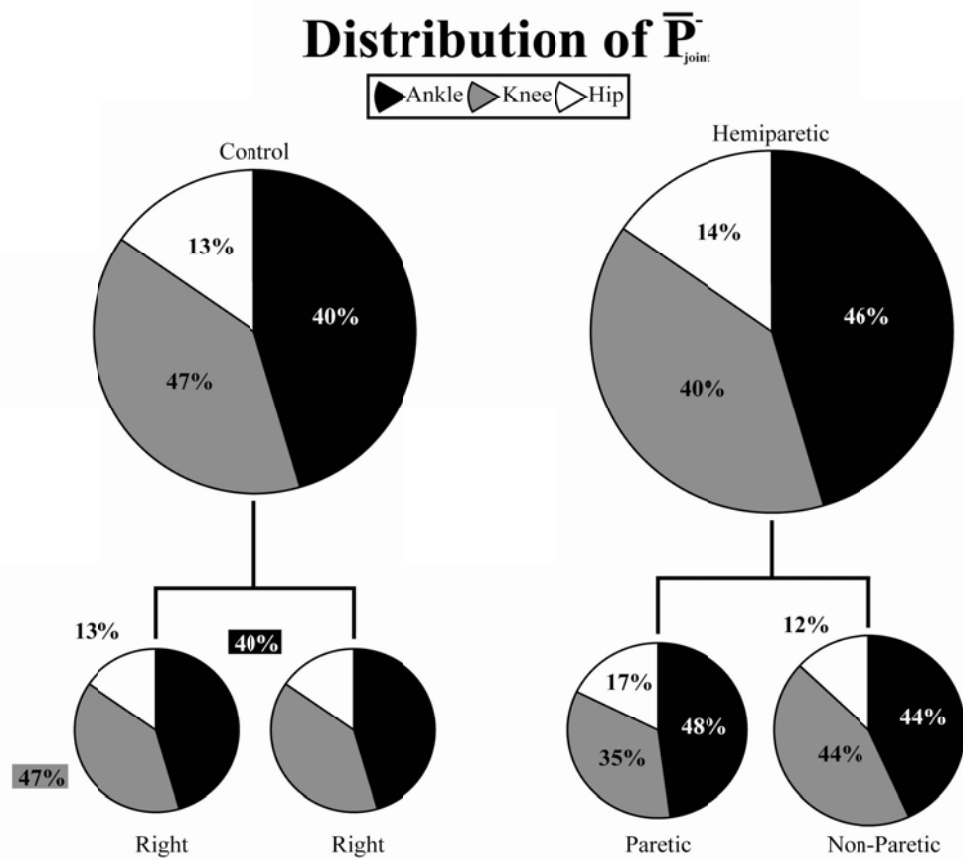


Figure 5: Net metabolic power (W kg^{-1}) (mean \pm sd) for unimpaired controls (white bar) ($n=9$) and post-stroke hemiparetic (gray bar) ($n=8$) participants during walking at 0.75 m s^{-1} . Asterisk indicates significant difference between hemiparetic and control ($p<0.05$).

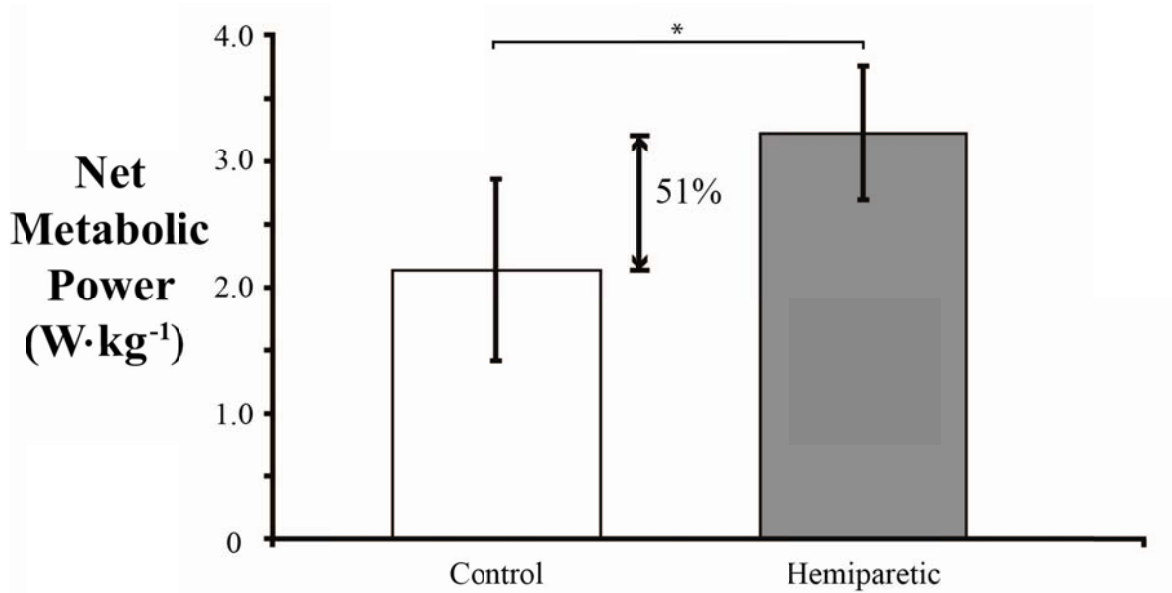


Figure 6: Placement of the ultrasound probe over the muscle belly of the medial gastrocnemius muscle. The pennation angle θ is defined as the angle between digitized fascicle and the superficial aponeurosis; L_{DF} is the length of the digitized fascicle; L_{SEE} is the length of the series elastic element – i.e. Achilles tendon (AT); L_{MTU} is the length of the MG MTU; SA is the superficial aponeurosis; DA is the deep aponeurosis; US is the ultrasound probe; SOL is the soleus muscle of the triceps surae

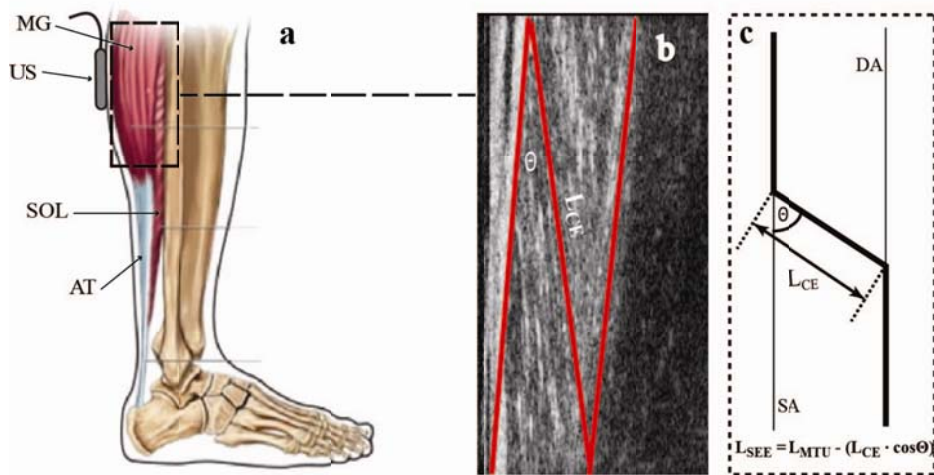


Figure 7: Ankle powers (W kg^{-1}), moments ($\text{N}\cdot\text{m kg}^{-1}$), and angular velocities (degrees sec^{-1}) for the paretic (dark solid green line), non-paretic (dark green dashed line), and control (light green solid line) limbs over a full stride.

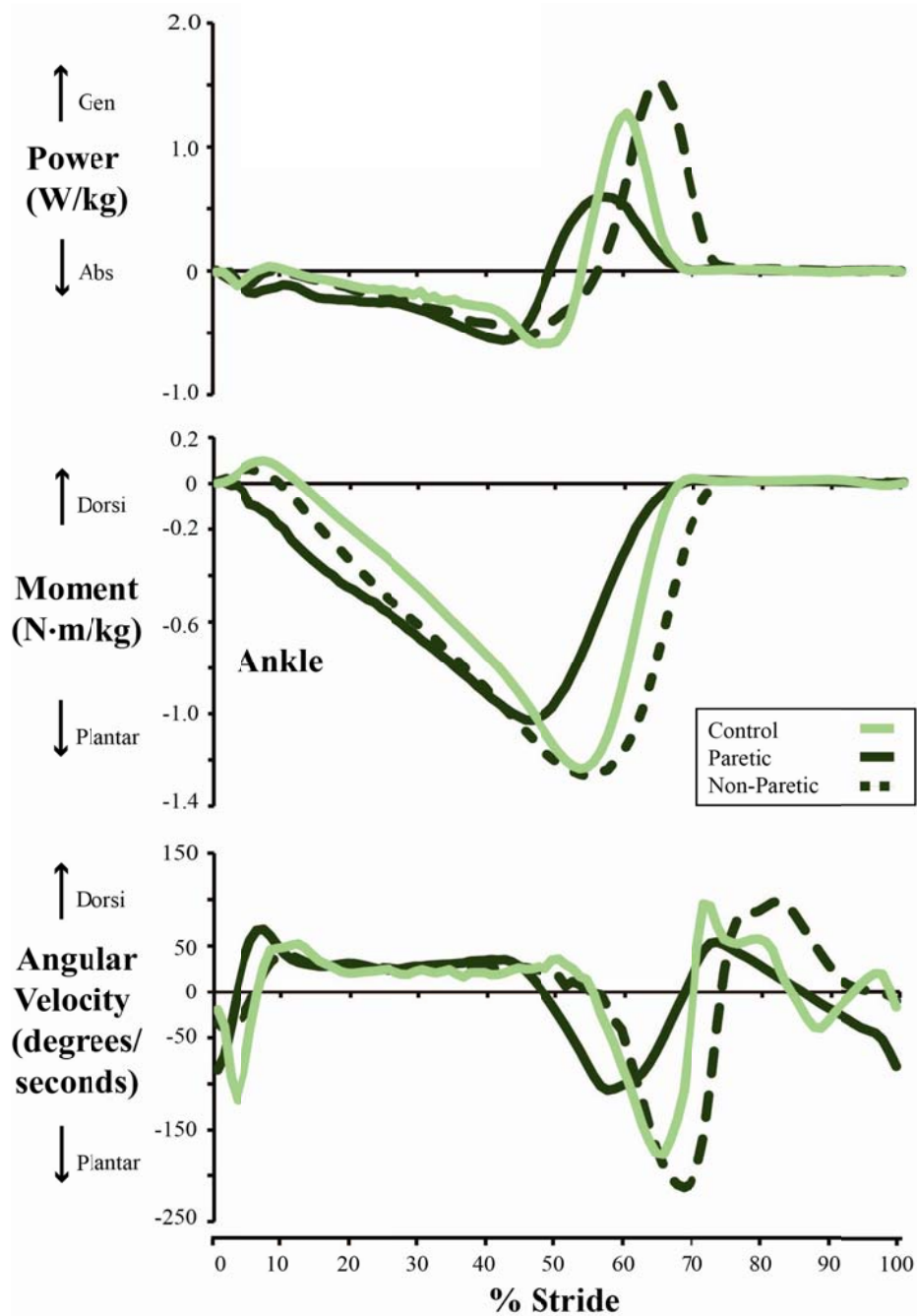


Figure 8: Length-change patterns (mm) of a unimpaired control muscle-tendon unit (MTU), fascicle (CE), and series elastic element (SEE). Light green represents the MTU, light red represents the CE and the light blue represents the SEE.

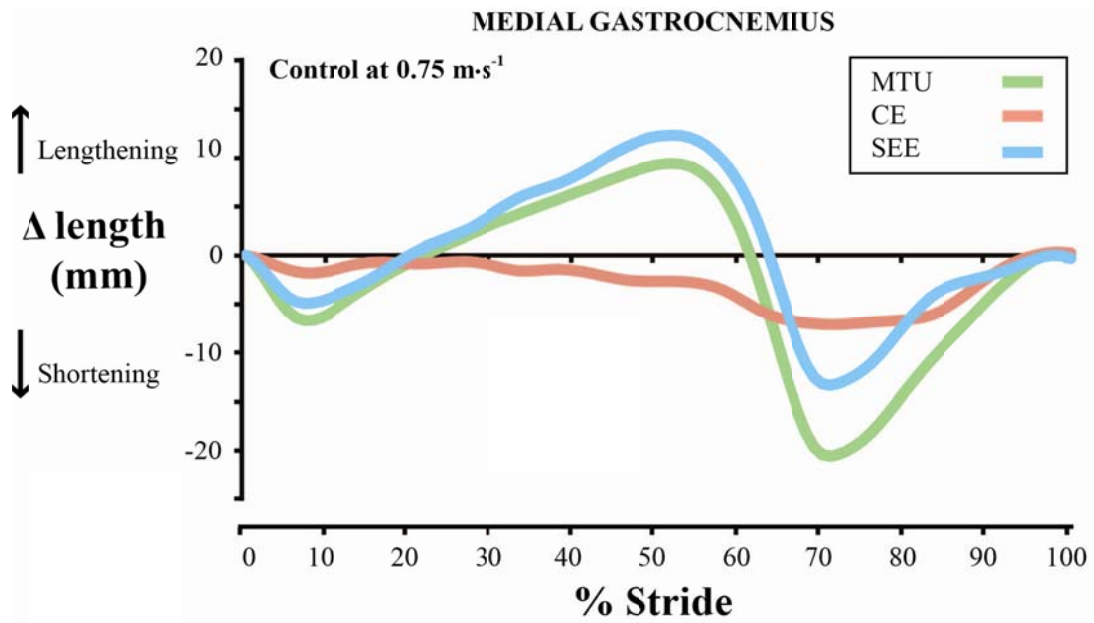


Figure 9: Length-change pattern (mm) of the MTU, CE and SEE for the paretic, non-paretic and control MG. The curves are grouped by the muscle fascicle MTU component. The green represents the MTU, red represents the CE, and the blue represents the SEE. The solid lighter line represents the control MG, the darker solid line represents the paretic MG, and the dashed darker line represents the non-paretic MG.

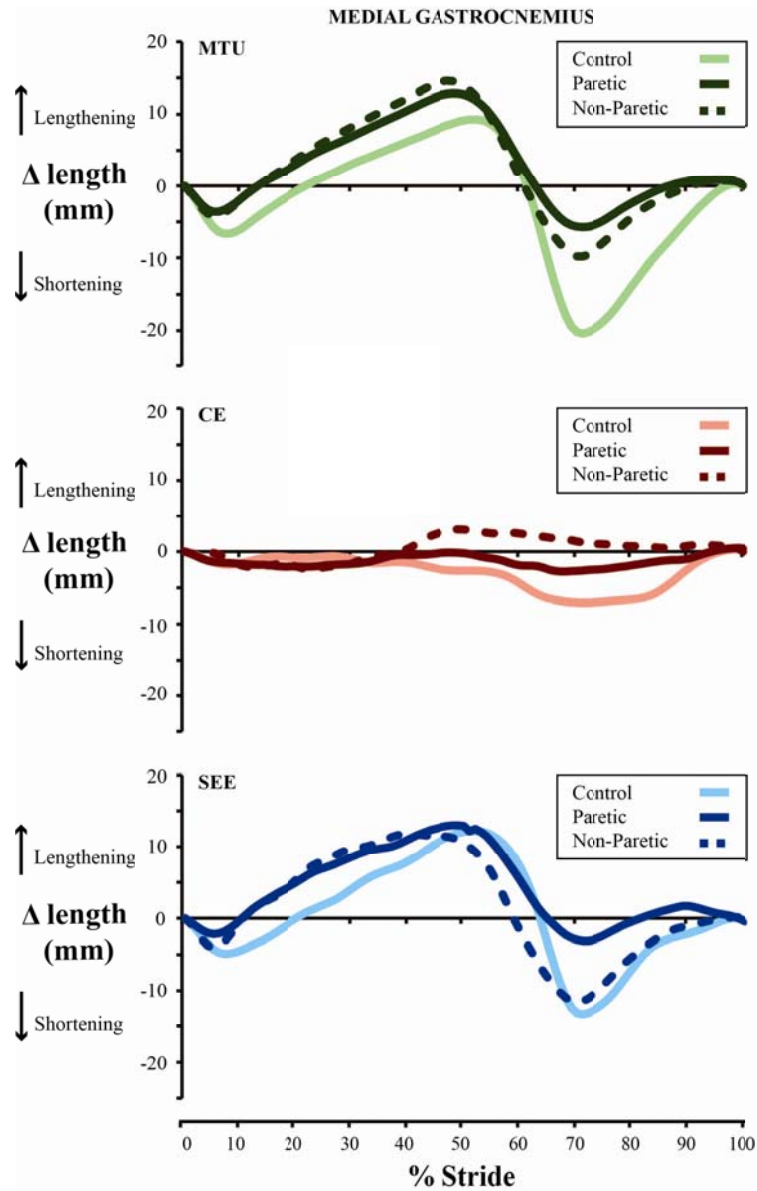


Figure 10: Force (N), velocity (mm s^{-1}) and power (W) of the MTU, CE and SEE for the control, paretic and non-paretic MG. Panels A-C show the MTU force, velocity, and power (shown in green); panels D-F show the CE force, velocity and power (shown in red), and panels G-I show the SEE force, velocity, and power.

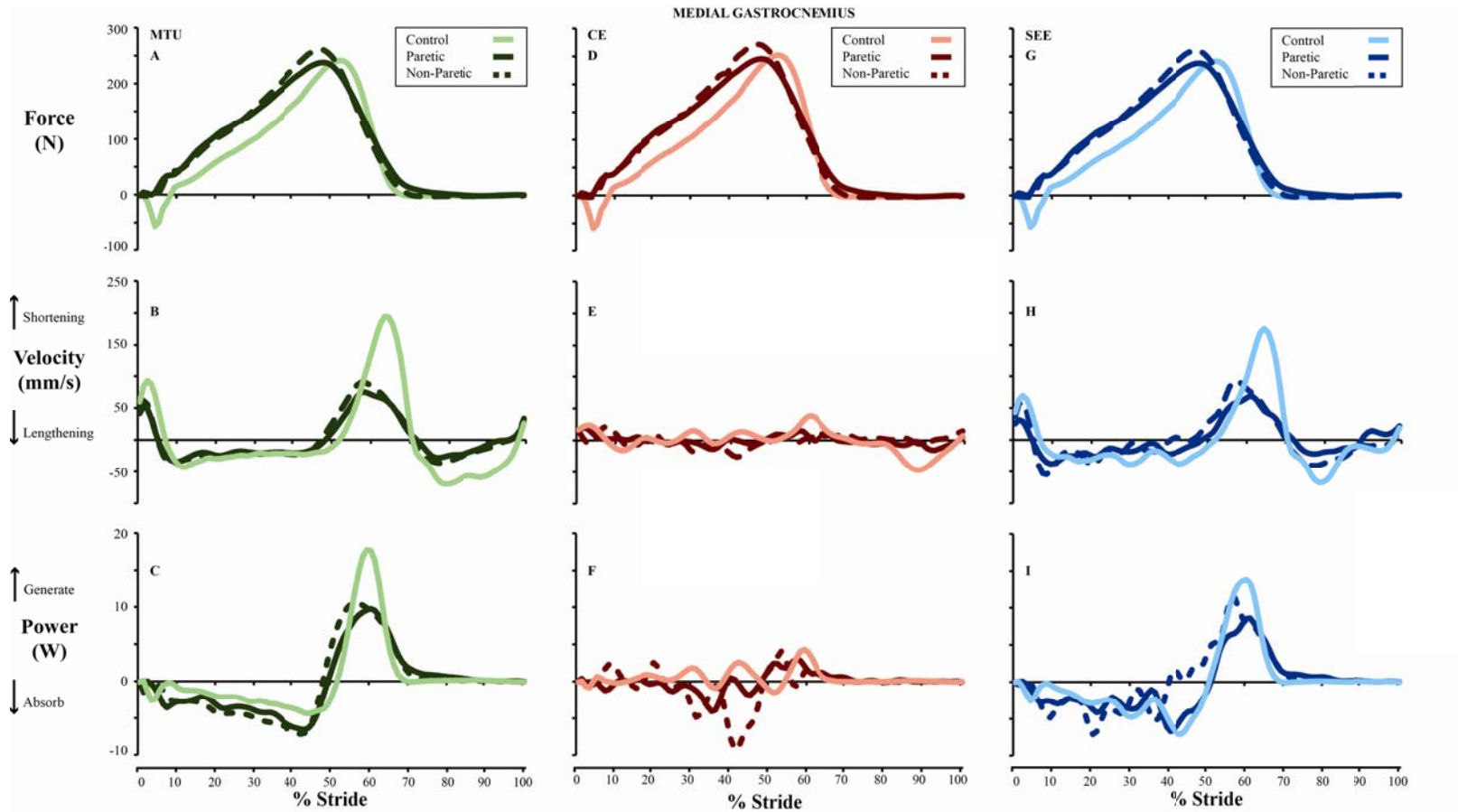


Figure 11: Average combined positive and negative power (W) for the CE and the SEE of the control, paretic and non-paretic limb. The red shows the CE power contributions, where as blue represents the SEE contributions. Statistical significance is noted by: * = paretic different than control; # = non-paretic is different than control ($p < 0.05$).

